

Heat and temperature distribution in a cladding-pumped, Er: Yb co-doped phosphate fiber

Cite as: Review of Scientific Instruments **75**, 5166 (2004); <https://doi.org/10.1063/1.1818591>
Submitted: 21 June 2004 . Accepted: 29 August 2004 . Published Online: 10 November 2004

Andrey Kosterin, J. Kevin Erwin, Mahmoud Fallahi, and Masud Mansuripur



View Online



Export Citation

ARTICLES YOU MAY BE INTERESTED IN

[Upconversion emission in Er-doped and Er/Yb-codoped ferroelectric \$\text{Na}_{0.5}\text{Bi}_{0.5}\text{TiO}_3\$ and its temperature sensing application](#)

Journal of Applied Physics **116**, 014102 (2014); <https://doi.org/10.1063/1.4886575>

MCL
MAD CITY LABS INC.

AFM & NSOM Nanopositioning Systems Micropositioning Single Molecule Microscopes

Heat and temperature distribution in a cladding-pumped, Er: Yb co-doped phosphate fiber

Andrey Kosterin,^{a)} J. Kevin Erwin, Mahmoud Fallahi, and Masud Mansuripur
Optical Sciences Center, the University of Arizona, Tucson, Arizona 85721

(Received 21 June 2004; accepted 29 August 2004; published 10 November 2004)

High-gain-per-unit-length, Er: Yb co-doped, phosphate glass fibers are a new class of active photonic materials. Due to their high concentration of active ions (typically $2-6 \times 10^{20} \text{ cm}^{-3}$), the generation of heat in these materials is rather severe. To facilitate the design of cladding-pumped, high-power lasers and amplifiers using these materials, we introduce two diagnostic techniques for measuring the total heat and the profile of temperature distribution along the length of an active fiber. Thermal experiments on a 6.0-cm-long piece of cladding-pumped phosphate fiber with Er: Yb doping (3:16 wt %) are conducted, and the results are compared with indirect estimates of total heat by scattered light measurements using a power-balance argument. The difference between the two methods is about 8.0%. Even at low pump powers, the temperature of the core (without heat-sinking) is found to be a large fraction of the glass transition temperature. The temperature distribution along the length of the fiber is found to be relatively flat compared with the absorption profile. Our thermal diagnostic tools yield valuable information that can be used to optimize the design of fiber lasers and amplifiers. © 2004 American Institute of Physics.

[DOI: 10.1063/1.1818591]

I. INTRODUCTION

Scaling of fiber lasers and fiber amplifiers to high power and the reduction of component size for efficient integration has brought attention to a new class of active materials; namely, the class of high-gain-per-unit-length Er: Yb co-doped phosphate glass fibers. Advantages of these materials include high phonon energy, high solubility of rare-earth ions (without clustering), and low cooperative upconversion.¹ One of the problems associated with these high-gain/length amplifiers is their large volume of dissipated heat, which results in elevated core temperatures within the active fiber. High core temperatures, in turn, adversely affect the amplifier efficiency and may ultimately cause thermal damage and catastrophic breakdown. That is one reason that fiber laser/amplifier designers need the results of accurate thermal measurements for information concerning dissipated heat and temperature distribution along the length of active fibers. The design of such devices is currently hampered by a lack of sufficient information concerning the thermal parameters, and by the absence of reliable methods for thermal characterization of active fibers.

In the recent past, thermal aspects of cladding-pumped fiber lasers have been studied by theoretical means. A comprehensive study was conducted for silicate fibers pumped at $\lambda_{\text{pump}}=915 \text{ nm}$ and lasing at $\lambda=1120 \text{ nm}$.² It was determined that, under operational conditions, the core center of the active fiber could reach a substantial fraction of the silicate material's melting temperature. Useful as such model calculations may be, they suffer from simplified assumptions such as uniform heat deposition along the length of the fiber, and

the assumption of material homogeneity in the core and cladding regions. Methods of heat and temperature measurement in active fibers are thus needed to verify these models and to extend their domain of application.

In the case of phosphate glass optical amplifiers, pumped at $\lambda_{\text{pump}}=976 \text{ nm}$ and lasing at $\lambda=1535 \text{ nm}$, the problem of heat dissipation within the fiber is even more severe than for silicate fibers because of higher quantum defect (0.368 as opposed to 0.183), higher active ion concentrations, and much lower melting temperatures. Investigations of thermal effects in these materials have been reported in the literature.^{3,4} In particular, the temperature of a disk-shaped optical amplifier has been determined by spectroscopy using upconversion emission intensity;³ the use of this technique for temperature sensing has been reported elsewhere.⁵⁻⁷ In contrast, for fiber-shaped high-gain/length phosphate glass materials, the thermal effects are largely unknown. Specifically, the core temperature distribution along an active fiber as well as methods of measuring such thermal profiles have not been reported.

In this article, we address the problems of heat dissipation and optical-thermal power balance in a cladding-pumped phosphate fiber, presenting two techniques for measuring the total heat and the core temperature distribution in such fibers. In Sec. II we describe our custom-built, oil-based calorimeter for measuring the total heat dissipated within a short length of an active fiber. A 6.0 cm piece of cladding-pumped Er: Yb (3:16 wt %) co-doped phosphate fiber is used in these experiments. In Sec. III we present the methodology of determining the core temperature profile as well as our experimental data along the length of the aforementioned fiber. Upconversion, usually considered a parasitic effect that limits the gain of fiber amplifiers, is used here to

^{a)}Electronic mail: akosterin@thermawave.com

monitor the core temperature. In Sec. IV we discuss the merits and demerits of our proposed heat and temperature diagnostic tools, compared with other available techniques. Implications of these techniques and recommendations for future work will also be discussed.

II. MEASUREMENT OF TOTAL HEAT

The heat dissipated in a length of active fiber can be measured by transient calorimetry. Conceptually, this technique is similar to the transient hot-wire method commonly used for measuring the thermal conductivity of liquids.⁸ In our technique, the wire as heating element is replaced with a short piece of an active, double-clad fiber. The active fiber is spliced on either end to a piece of passive, double-clad fiber, which provide the means for end-pumping the active fiber from one end, and measuring the transmitted light at the opposite end. The active segment of the aforementioned chain is placed inside an 8-cm-long, 9-mm-diameter quartz tube filled with a heat-absorbing fluid. The quartz tube, equipped with thermocouples that are immersed in the fluid, is housed within an evacuated chamber to minimize heat loss to the outside world. A source of pump light ($\lambda_{\text{pump}} = 976$ nm) is attached to one arm of the fiber chain, while the other arm is connected to a power meter. The heat dissipated in the active fiber diffuses through the fiber–fluid interface to the fluid (convection and radiation processes are neglected), thus raising the fluid’s temperature. The thermocouples measure the temperature of the fluid as a function of time. Assuming “instant” thermal conductivity of the fluid, the total thermal power at time t_0 (when the heating begins) can be calculated as follows:

$$P = c_p m \left(\frac{dT}{dt} \right) \Big|_{t_0}. \quad (1)$$

Here, c_p is the specific heat, m the mass, and T the temperature of the fluid.

The calorimeter is shown in Figs. 1(a) and 1(b), and its schematic diagram appears in Fig. 1(c). The test fiber is a chain consisting of two pieces of passive, double-clad silica fiber fusion-spliced to the two ends of a short, double-clad, active phosphate fiber. The chain is placed in the middle of a quartz tube filled with oil. The 8-cm-long, 9-mm-diameter tube (wall thickness=1 mm) was cut open at the top to provide a slit for inserting the fiber. TKO-19+ oil (Kurt J. Lesker Co.), a low-vapor pressure fluid, was used as the heat-absorbing medium. Three type-K thermocouples were inserted from the bottom of the tube with their sensitive areas located halfway between the fiber and the cell wall. [For simplicity, only the central thermocouple is shown in Fig. 1(c); the other two were equally spaced, 10 mm apart on either side of the central thermocouple.] Depending on the pump absorption distribution along the active fiber, one or another thermocouple could provide the best measurement of the oil temperature. In preparation for thermal measurements, 2.5 cm³ of oil was poured over the fiber chain. The chamber was evacuated to 160 Torr, and the temperature data from the thermocouples were stored in a computer. To characterize the vacuum fluid, we measured its thermal prop-

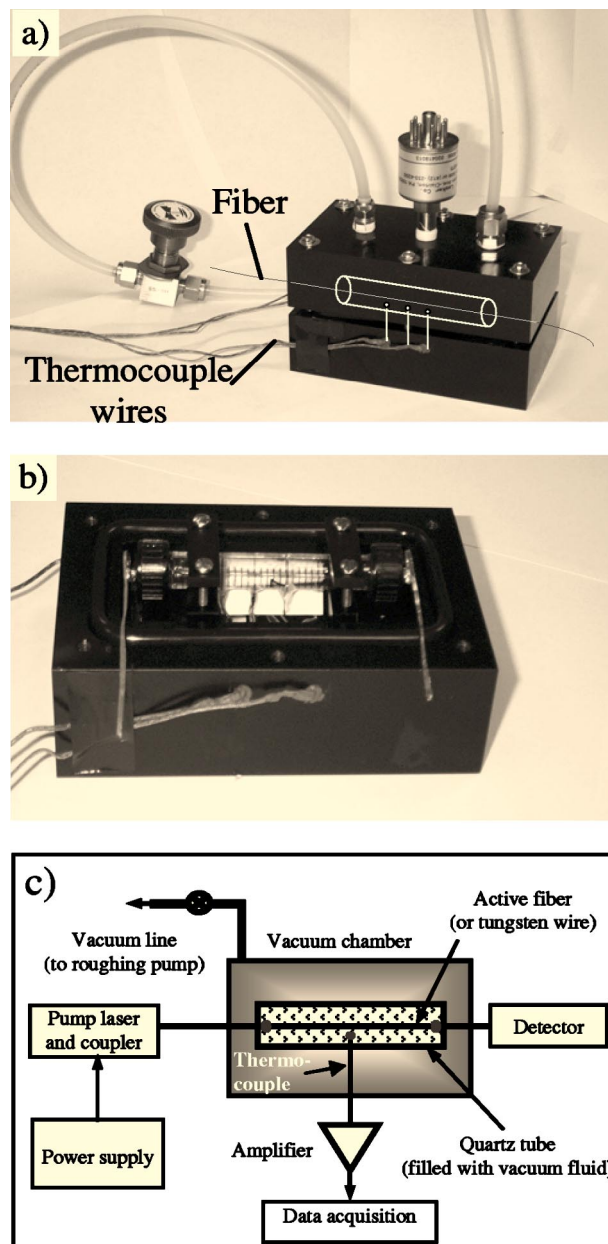


FIG. 1. (a) Photograph of the calorimeter, showing the connections to the vacuum pump and the vacuum gauge. The optical fiber (or the tungsten wire) entering the chamber and the thermocouple wires are visible outside the chamber. Superimposed on the photograph is a diagram showing the quartz housing of the fiber (inside the vacuum chamber) with three thermocouples inserted. (b) Photograph of the calorimeter with the cover plate removed. The oil-filled quartz tube and the copper wires that feed the tungsten wire are clearly visible in this picture. (c) Schematic diagram of the calorimeter.

erties using a modulated differential scanning calorimeter (MDSC 2920, TA Instruments Inc.); the fluid’s constants thus obtained are listed in Table I. We also checked the spectral properties of the fluid to ensure that no light absorption takes place near $\lambda = 550, 976,$ and 1535 nm, which are the relevant wavelengths of scattered light in our experiments. Diffusion of heat from the fiber is thus assumed to be the dominant heating mechanism; all radiation coming into the oil from scattering pump and amplified spontaneous emission can be ignored.

In practice, of course, the oil’s thermal conductivity is

TABLE I. Characteristics of vacuum fluid TKO-19+ at room temperature.

Density	ρ	0.872	g/cm ³
Thermal conductivity	K	0.15	W/m/K
Thermal diffusivity	α	1.01×10^{-7}	m ² /s
Specific heat	C_p	1.7	J/g/K

not infinite, which places a lower limit on the beginning moment for data acquisition. The heat wave reaches the thermocouple in $t=r^2/\alpha$, where $r \sim 1.75$ mm is the separation between the thermocouple and the fiber, and α is the thermal diffusivity of the oil (see Table I). Therefore, the data acquisition must begin at $t_0 \sim 30$ s (we collected data starting at $t=0$, but processed them only after $t=30$ s.) The estimated Fourier number of $F=840$ for the fiber ($F=pt/a^2$, where ρ is the radius of the fiber) shows that in 30 s the heat propagates far from the fiber–oil interface and, therefore, the thermal properties of the fiber can be ignored.

The calorimeter measurements resulted in sets of transient temperature curves; the time interval between sampling points for the thermocouples was 30 s. Initially, the curves were linear with slopes determined solely by the heating power of the fiber. The sensitivity, defined as the minimal measurable slope of 0.1 °C over four sampling points, was $\sim 6.3 \times 10^{-4}$ °C/s. The maximal slope of 6.7 °C/s was estimated based on the fluid’s flash point.

Pump light from a multimode diode laser ($\lambda_{\text{pump}}=976$ nm, power=1.5 W) was side-coupled into the input arm of the fiber chain using a prism side-coupler (PCS Q048, NP Photonics, Inc.). The fiber chain was assembled from an active fiber and two pieces of double-clad passive silica fiber, each 50 cm long, with the core/clad1/clad2 diameters of 6/86/120 μm . Numerical aperture (NA) of the core/clad1 interface was 0.11, that of the clad1/clad2 interface was 0.22. The double-clad active segment was a 6-cm-long phosphate glass fiber doped with Er: Yb (3:16 wt %, NP Photonics). The corresponding active fiber diameters were 6/60/103 μm . Given the prism coupling, light with $\sim 25^\circ$ angular diameter full width at half-maximum propagated in the first cladding.

To calibrate the calorimeter, we replaced the fiber chain with a tungsten wire inside the quartz tube. The 8-cm-long, 180- μm -diameter wire had a room-temperature resistance $R_w \sim 0.18 \Omega$ (McMaster-Carr). A two-stage process was employed to account for the temperature dependence of R_w . In the first stage, with currents below ~ 2 A (i.e., low heating power), a constant wire resistance was assumed (zeroth-order approximation). The deposited heat power is given by $R_w i^2$, where R_w is the room-temperature wire resistance and i the electric current. The oil temperature T slowly increased with time, with a slope $\Delta T/\Delta t = \kappa R_w i^2 / Cm$, where C is the oil’s specific heat, m its mass, and κ a temperature reduction coefficient due to thermal conductivity ($\kappa \sim 0.33$ was measured for the oil cell). The resulting calibration plot shown in Fig. 2 (●) shows the heating power versus the measured temperature slope. The predicted power versus slope is a linear curve in this approximation.

At higher powers the wire resistance increases percepti-

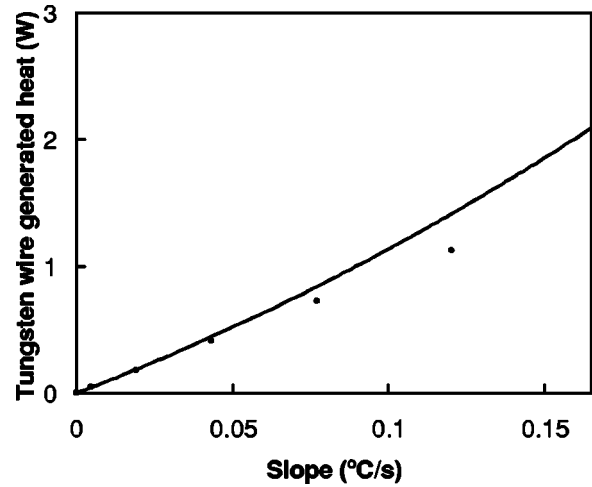


FIG. 2. Calorimeter calibration curve obtained with a tungsten wire. Solid circles (●) represent the measured heat generated in the wire based on the assumption that the wire’s resistance is independent of its temperature (zeroth-order approximation). The solid curve is the result of calculations based on an analytical model that accounts for the wire resistance’s temperature dependence.

bly with the temperature, and the dissipated heat power (to a first-order approximation) may be described by its average value $i^2 \tilde{R}_w = i^2 R_0 (1 + \beta \Delta \tilde{T})$, where \tilde{R}_w is the average wire resistance for the period of measurement, R_0 is the wire resistance at $T=0$ °C, and β is tungsten resistance’s temperature coefficient (0.0051 °C⁻¹). Assuming a measurement period τ equal to four sampling intervals (120 s), and that the temperature rise is approximately linear, the average temperature is given by $\Delta \tilde{T} = 1/\tau \int_0^\tau \Delta T dt$, with $\Delta T = (q/4\pi K) \ln(4\alpha t/r^2 C)$, where $q = R_w i^2 / l$ is the heat linear density (zeroth-order approximation), K and α are the thermal conductivity and diffusivity of the oil, respectively, r is the radius of the wire, $C=1.781$, and t is the time after the start of heating.⁹ The corrected calibration plot, the solid curve in Fig. 2, thus accounts for the temperature dependence of the wire’s resistance.

Returning now to the thermal measurements with the fiber chain, the experimentally measured plots of transient temperature versus time for various input pump powers are plotted in Fig. 3. Subsequently, with the aid of the calibration plot in Fig. 2, the slopes of these curves at $t=t_0$ were used to estimate the dissipated heat. Figure 4, open circles (○), show, as a function of the injected pump power, the total dissipated heat in the active fiber. One important observation is that the dissipated heat is a large fraction, nearly 60%, of the input pump power.

III. TEMPERATURE DISTRIBUTION ALONG THE LENGTH OF THE FIBER

The temperature of the core is a limiting factor in scaling up the power of cladding-pumped fiber lasers and amplifiers. In general, the temperature profile along the length of the active fiber is expected to be nonuniform (because of a short pump-absorption length) and also to be dependent upon the specific geometry used to deliver the pump light to the fiber. For proper management of the active fiber’s temperature dur-

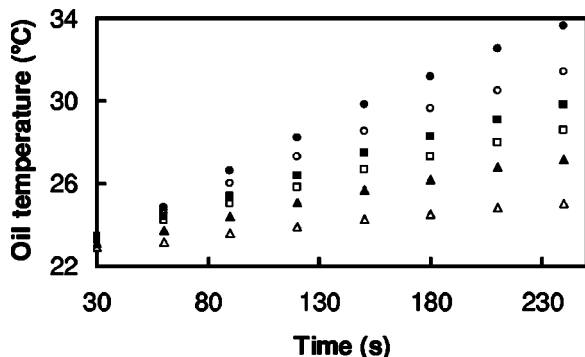


FIG. 3. Results of transient heat measurements (using the calorimeter) for a 6.0-cm-long piece of active fiber. Shown are plots of the oil temperature versus time for several pump powers P : (●) $P=1330$ mW; (○) $P=867$ mW; (■) $P=712$ mW; (□) $P=557$ mW; (▲) $P=403$ mW; (△) $P=248$ mW.

ing operation (i.e., design of an effective cooling system, the temperature distribution along the core must be taken into account.

In principle, visual information on the fiber core's temperature distribution can be provided by a thermal imaging camera operating in the $3\text{--}5\ \mu\text{m}$ or $7.5\text{--}13\ \mu\text{m}$ sensitivity windows.¹⁰ However, cameras generally provide temperature images by assuming black-body emissivity for the test object and, when fiber emissivity deviates from that of a black body, the images thus obtained can be interpreted only qualitatively. Alternative techniques are therefore desirable for fiber core temperature assessment. Temperature sensors that rely on the specific properties of rare-earth-doped glasses are good candidates for this application and, indeed, accurate measurements can be obtained for high concentration Er: Yb co-doped fibers using upconversion fluorescence emission in the green wavelength range $520\text{--}550\ \text{nm}$.

In high-gain/length fiber amplifiers, upconversion is usually a parasitic, gain-limiting factor. At high pump powers, upconversion results in strong fluorescence emission along the length of the active fiber. Using a small-area detector, we collected the emitted green light immediately outside the cladding as a function of the position along the fiber's length. As will be explained below, the spectrum of this light con-

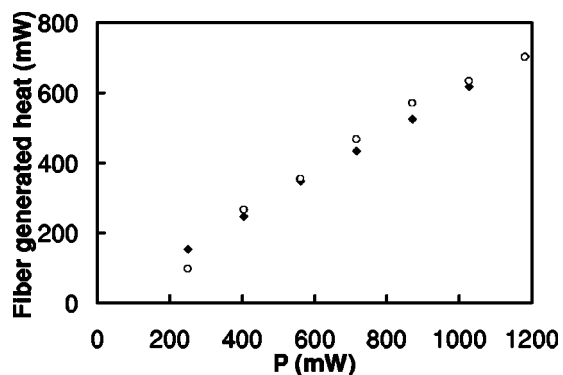


FIG. 4. Total heat generated in the fiber versus the pump power P . The open circles (○) represent the heat measured directly using the calorimeter. The solid diamonds (◆) show the estimated heat based on a power balance argument that accounts for the loss of pump light due to transmission through the fiber as well as loss by scattering.

tains sufficient information to enable one to extract the local temperature of the fiber's core. For calibration we used a procedure based on measuring upconversion spectra in the limit of zero pump power.

A. Experimental procedure

The core temperature of the active fiber was estimated from the spectral properties of the fluorescent green light collected outside the fiber. The source points located in the core were geometrically conjugated by imaging optics with the slit of a spectrometer. The optical system consisted of a $40\times$ microscope objective ($\text{NA}=0.6$) for coupling the emitted light into a delivery fiber (2-m-long, multimode AFS 105/125 Y fiber), and an imaging lens ($F\#2$, 5 cm focal length) for projecting the output of the delivery fiber onto the slit of the spectrometer. The detection system consisted of a 0.22 m spectrometer (EG&G PARC Model 1681) equipped with a 1472 photomultiplier tube with a spectral resolution of 0.5 nm. To measure the fiber's temperature profile, the core was scanned using a micrometer screw with a 5 mm step, as shown in Fig. 5(a). The Er: Yb co-doped phosphate fiber was cladding pumped at $\lambda\sim 976\ \text{nm}$ using a 2 W prism-coupled laser diode (PCS Q048, NP Photonics, Inc.); the (nonuniform) absorption of the pump within the core was the only source of heat during our measurements.

Information about the core temperature is contained in the intensity ratio of two thermally coupled energy levels of Er^{3+} ions excited by the upconversion mechanism. (This method of measurement was originally demonstrated by Berthou and Jorgensen with fluoride glass;⁵ their technique automatically accounted for the excitation power noise.) Typical spectra of the upconverted light from the double-clad fiber described in Sec. II are shown in Fig. 5(b); the solid circles (●) correspond to the pump launch position at $x=0$, while the open circles (○) represent the midpoint of the fiber (pump power $\sim 1175\ \text{mW}$). The central wavelengths of the two bands (calculated by weighted averaging of each line) were found to be $\lambda_{31}=526\ \text{nm}$ and $\lambda_{21}=547\ \text{nm}$, corresponding, respectively, to Er^{3+} transitions from ${}^2H_{11/2}$ (level 3) and ${}^4S_{3/2}$ (level 2) to the ${}^4I_{15/2}$ ground state (level 1). In the upper plot of Fig. 5(b), the I_{31} band is stronger than the I_{21} band, whereas in the lower plot the two bands are nearly equal in strength. The ratio $R=I_{31}/I_{21}$ of the emission intensities at the central wavelengths of the two bands is solely dependent on the local core temperature. The fact that this ratio differs for the two plots of Fig. 5(b) thus indicates the presence of a temperature gradient along the length of the fiber.

For a quantitative analysis, we describe briefly the excitation mechanism responsible for the upconversion emission. The absorption of the pump photons excites the Yb ions to the ${}^2F_{5/2}$ metastable state.¹⁰ The excited Yb ions transfer their energy (nonradiatively) to the nearest Er ions, thus exciting them to the ${}^4I_{11/2}$ state. These Er ions are further excited to the ${}^4F_{7/2}$ level via energy transfer from other neighboring Yb ions (${}^2F_{5/2}$). Levels 3 and 2 are then populated by relaxation from the ${}^4F_{7/2}$ states, and settle into a quasithermal equilibrium.^{3,11} The ratio R of the emission intensities from levels 3 and 2 in the green upconversion signal is given by

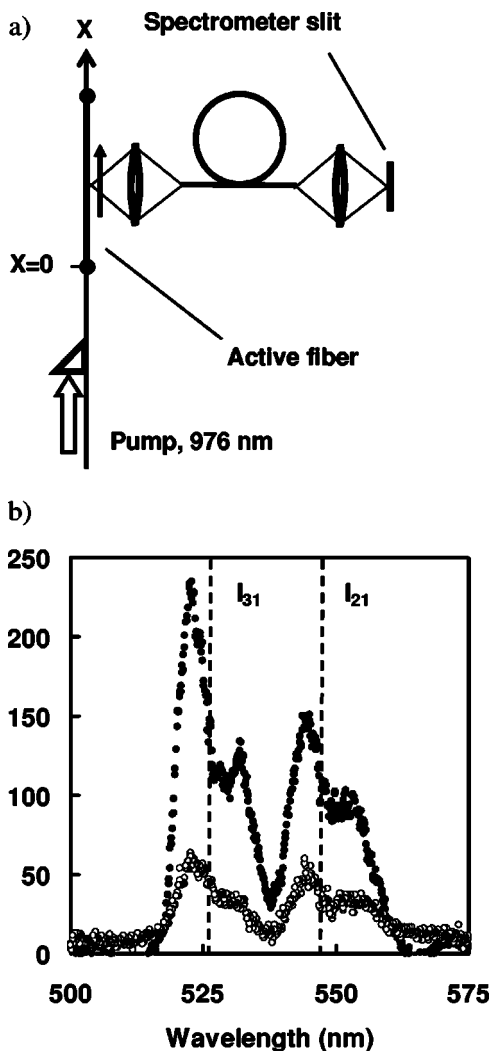


FIG. 5. (a) Diagram of the setup used for measuring temperature distribution along the length of an active fiber. The upconverted light is collected and fed to a spectrometer by means of two lenses and a piece of multimode fiber between the lenses. (b) Upconversion emission spectra measured at two different locations along the fiber. The solid circles (●) correspond to the pump launch position at $x=0$, whereas the open circles (○) represent the midsection of the fiber at $x=30$ mm.

$$R = C \exp\left(-\frac{\Delta E_{32}}{kT}\right), \quad (2)$$

where ΔE_{32} is the energy gap between the levels, k is the Boltzmann constant, T is the absolute temperature, and the coefficient C is given by Shinn *et al.*:¹¹

$$C = \frac{c(\nu_3)A_3g_3h\nu_3}{c(\nu_2)A_2g_2h\nu_2}. \quad (3)$$

Here, c is the response of the detector, $\nu_{2,3}$ are the transition frequencies, $g_{2,3}$ are the level degeneracies ($2J+1$), $g_3/g_2=3$, and $A_{2,3}$ are the rates of spontaneous emissions. (The spontaneous emission rates for our phosphate glasses are not presently available; they can be measured or calculated phenomenologically using the Judd–Ofelt theory.)

The C coefficient in Eq. (2)—and, by implication, the ratio of the spontaneous emission rates—is obtained by measuring $R(T)$ in the limit of zero pump power. The fiber chain used in our experiments has been described in Sec. II. Since

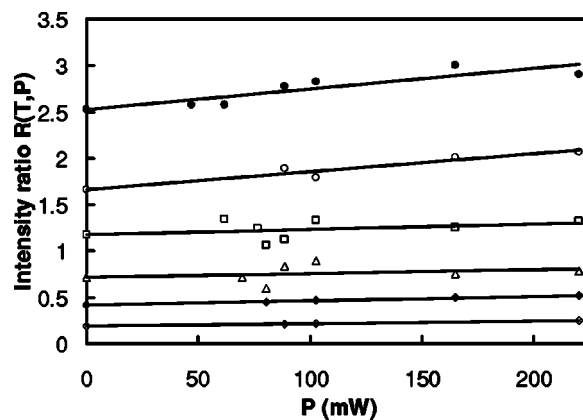


FIG. 6. Upconversion intensity ratio $R(T,P)$ versus the pump power P at various ambient temperatures T : (●) $T=773$ K; (○) $T=633$ K; (□) $T=513$ K; (△) $T=413$ K; (◆) $T=353$ K; (◇) $T=296$ K. The true $R(T)$, as described by Eq. (2), is obtained in the limit when P approaches zero, that is, $R(T)=\lim_{p \rightarrow 0} R(T,p)$.

the pump ($\lambda=976$ nm, power= P) is the source not only for upconversion but also for heat generation in the active fiber, its power must be taken into account when measuring the material characteristic $R(T)$. To observe the effect of the pump power P on the intensity ratio $R(T)$, we placed the fiber chain in an oven set at different temperatures T ranging from 296 to 773 K, and varied the pump power P . Rather than attempting to detect the scattered green light outside the fiber, we collected the guided light in the reverse direction relative to the pump light, thus obviating the need for placing the optics in the oven (only the fiber chain was heated in the oven).

Measured plots of $R(T,P)$ versus P at several values of T are shown in Fig. 6. When these curves are extrapolated to zero pump power, the true values of $R(T)$ are obtained. (The dependence of R on pump power P was investigated by dos Santos *et al.*,⁶ who reported a constant R for powers up to $P \sim 200$ mW in the temperature range 293–523 K, and a slight increase of R at $P > 200$ mW. Our measurements, however, indicate that R is a monotonically increasing function of P , with a slope that is larger at higher temperatures T .)

Figure 7 is a plot of the measured $R(1/T)$ on a semilogarithmic scale; the best linear fit to this curve is $\ln R = -1195.5(1/T) + 2.5156$. The measured coefficients fully determine the peak’s intensity ratio R as a function of

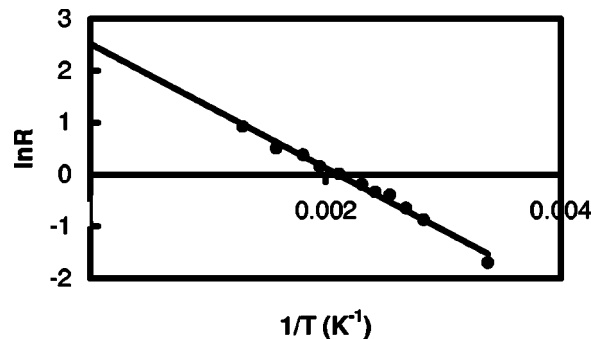


FIG. 7. Plot of the measured $R(1/T)$ on a semilogarithmic scale; the best linear fit to this curve is $\ln R = -1195.5(1/T) + 2.5156$.

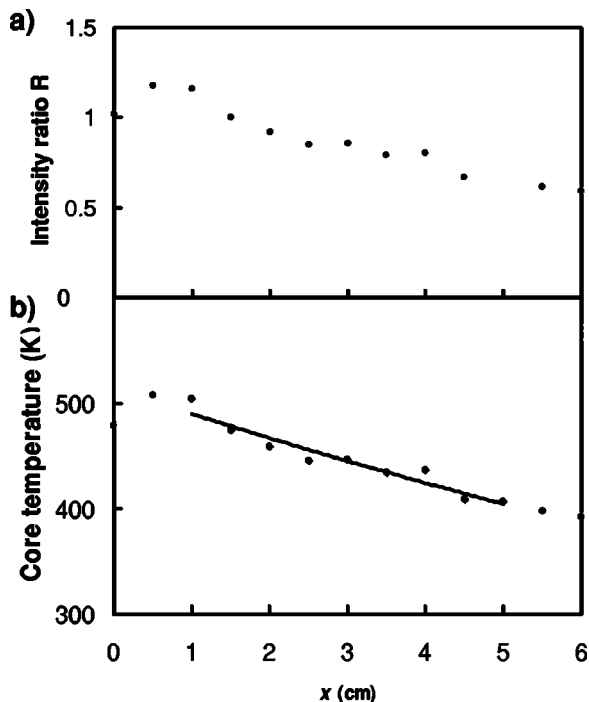


FIG. 8. (a) Measured upconversion intensity ratio R versus the distance x along the length of the fiber; the pump launch position is at $x=0$. (b) Estimated fiber core's temperature distribution along the length of the fiber. The solid curve, a fit to the measured temperature profile in the fiber's midsection, is not affected by the conditions at the end points, where the pump light enters and exits the fiber.

temperature T . Using these coefficients, the values of $\Delta E_{32}=829.5 \text{ cm}^{-1}$ and $A_3/A_2=3.97$ were obtained for our phosphate glass. Equation (2) can then be employed to determine the fiber's temperature.

B. Results

Using the system depicted in Fig. 5(a) we measured the temperature distribution along the length of an active fiber. At $P=1176 \text{ mW}$, the measured ratio R of the peak intensities versus the position x along the fiber is plotted in Fig. 8(a). Using Eq. (2), we converted the measured intensity ratio to the absolute temperature of the core; the results are shown in Fig. 8(b). The plot of core temperature versus position shows a nonuniform distribution, with the maximum temperature occurring at $\sim 7 \text{ mm}$ from the launch point. The temperature at $x=0$ (the launch point) is $\sim 33^\circ$ below the maximum value, perhaps because of the thermal conduction along the fiber. Away from the launch boundary, the temperature drops rather monotonically; the solid curve in Fig. 8(b) is the best fit to the data in the midsection of the fiber. The hottest and coldest points along the length of the fiber are 218 and 99 K above the ambient temperature ($T_{\text{ambient}}=296 \text{ K}$). It is thus seen that, even at moderate pump powers, the core temperature can reach a substantial fraction of the (phosphate) glass's transition temperature ($T_g=843 \text{ K}$).

IV. DISCUSSION

In the preceding sections we described two diagnostic techniques for thermal characterization of highly doped,

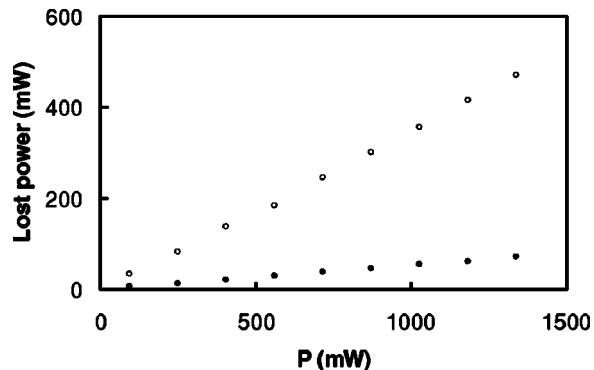


FIG. 9. Measured loss of the pump light versus the input pump power P . Open circles (○) show the loss caused by transmission through the fiber, whereas solid circles (●) represent loss by scattering. The data is used in power-balance calculations where the input optical power minus the lost optical power should be equal to the heat dissipated in the fiber's core.

cladding-pumped phosphate fibers. Even though both techniques rely on direct, well-calibrated measurements, it seems reasonable to compare their results with other estimates of the thermal properties of the fiber.

For an independent estimate of the dissipated heat in the core, we use a power balance argument. This requires a knowledge of the total pump power launched, as well as the loss of pump power upon transmission through the cladding, and loss of pump due to various scattering mechanisms. The difference between the launched pump power and the optical power lost by the above mechanisms should be equal to the dissipated heat. The residual pump power that leaves the fiber chain unabsorbed was measured; the resultant pump power loss versus the launched power P is shown with open circles (○) in Fig. 9.

The scattered light at $\lambda=976 \text{ nm}$ and $\lambda=1535 \text{ nm}$ was also measured; the total loss due to these scatterings is shown in Fig. 9 as solid circles (●). For these measurements the fiber chain was placed inside a 10 W Spectrolon integrating sphere (Labsphere) equipped with a germanium detector (GDA-C CE). The fiber was bent slightly to prevent the scattered light from reaching the detector directly. To separate the scattered light of differing wavelengths, one measurement was done with a 1535 blocking filter (optical density =5) in front of the detector, and one without the filter. The scattered 1535 nm emission was found to be $\sim 1\%$ of the total pump loss. (No guiding of the 1535 nm light within the core was observed. We also ignored the weak loss at the upconversion frequencies because of the small cross sections for these effects.¹²)

The heat generated in the fiber is thus expected to be equal to the difference between the launched pump power and the power lost to transmission and scattering. The resultant heat estimated from this power balance argument is plotted versus the launched pump power P in Fig. 4, solid diamonds (◆). Fairly good agreement with the calorimetry data is obtained through the range of available pump powers. At the lowest pump power of $P=248 \text{ mW}$, the rather large difference between the two estimates is probably due to the error of calorimetric measurements, as this method approaches its limit of sensitivity at low pump powers.

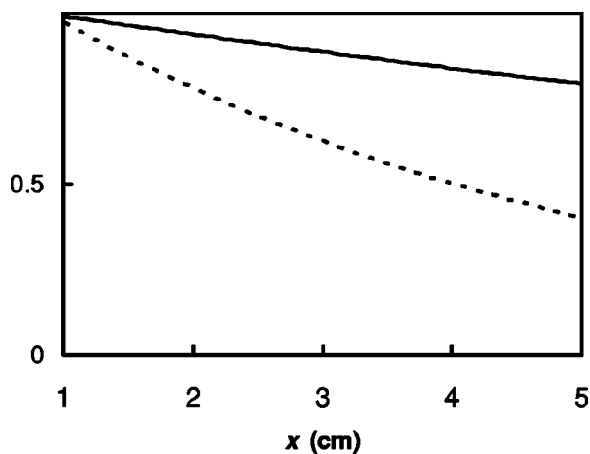


FIG. 10. The solid curve, reproduced from Fig. 8(b), is the profile of normalized temperature in the midsection of the fiber. The dashed curve shows the absorbed pump power (normalized) versus the position x along the fiber (courtesy of Dan Nguen, NP Photonics, Inc.). The absorbed pump power is obtained by computations based on the beam propagation method for the relevant experimental conditions.

In our direct measurements of the core temperature, we also attempted to raise the pump power (using a 20 W source) in order to determine the highest possible pump power without actively cooling the fiber. In two independent experiments, we observed an explosion of the fiber when the pump power was raised to ~ 3 W. Since our measurements at $P \sim 1.2$ W resulted in ~ 240 °C increase in core temperature, we expect a temperature rise of ~ 600 °C at $P = 3$ W, which is close to the glass transition temperature, $T_g = 570$ °C, of the phosphate glass (NP Photonics, Inc.) used in our experiments.

The measured temperature profile of the fiber shown in Fig. 8(b) can be compared with the distribution of the absorbed pump power calculated by a beam propagation

method code for the same experimental conditions. The theoretical results are shown in Fig. 10 as a dashed curve (courtesy of Dr. Dan Nguen, NP Photonics, Inc.), and compared with the normalized plot of the measured temperature in the midsection of the fiber (solid curve). The absorbed pump power is seen to drop with distance from the launch point faster than the temperature does; this is not unexpected, considering that thermal conduction spreads the heat along the fiber.

ACKNOWLEDGMENTS

Thanks are due to Shubin Jiang, Yushi Kaneda, Christine Spiegelberg, and Dan Nguyen of NP Photonics, Inc. for providing the active fibers used in our experiments, and for their participation in helpful discussions. This research was supported under AFOSR Contract No. F49620-02-1-0380 awarded by the Joint Technology Office.

- ¹Y. Hu, S. Jiang, T. Luo, K. Seneschal, M. Morrell, F. Smektala, S. Honkanen, J. Lucas, and N. Peyghambarian, *IEEE Photonics Technol. Lett.* **13**, 657 (2001).
- ²D. C. Brown and H. Hoffman, *IEEE J. Quantum Electron.* **37**, 207 (2001).
- ³Z. Cai, A. Chardon, H. Xu, P. Féron, and G. M. Stéphan, *Opt. Commun.* **203**, 301 (2002).
- ⁴N. V. Nikonorov, A. K. Przhnevskii, and A. V. Chukarev, *Proc. SPIE* **4282**, 219 (2001).
- ⁵H. Berthou and C. K. Jörgensen, *Opt. Lett.* **15**, 1100 (1990).
- ⁶P. V. dos Santos, M. T. de Araujo, A. S. Gouveia-Neto, J. A. Medeiros Neto, and A. S. B. Sombra, *IEEE J. Quantum Electron.* **35**, 395 (1999).
- ⁷D. N. Messias, M. V. D. Vermelho, and A. S. Gouveia-Neto, *Rev. Sci. Instrum.* **73**, 476 (2002).
- ⁸Y. Nagasaka and A. Nagashima, *Rev. Sci. Instrum.* **52**, 229 (1981).
- ⁹H. S. Carslaw and J. C. Jaeger, *Conduction of Heat in Solids*, 2nd ed. (Oxford University Press, Oxford, 1959).
- ¹⁰D. J. Coleman and T. A. King, *Meas. Sci. Technol.* **14**, 998 (2003).
- ¹¹M. D. Shinn, W. A. Sibley, M. G. Drexhage, and R. N. Brown, *Phys. Rev. B* **27**, 6635 (1983).
- ¹²Y. L. Lu, Y. Q. Lu, H. Fang, and N. B. Ming, *Opt. Commun.* **115**, 110 (1995).